TWO-LEVEL TUNNELING SYSTEM ANALYSIS USING BRILLOUIN SPECTROSCOPY

By Verenise Martinez Lopez

A Thesis

Submitted in Partial Fulfillment

of the Requirements for the Degree of

Master of Science

in Applied Physics

Northern Arizona University

May 2023

Approved:

Ryan Behunin, PhD., Chair

Christopher Mann, PhD.

Angel Martinez, PhD.

ABSTRACT

TWO-LEVEL TUNNELING SYSTEM ANALYSIS USING BRILLOUIN SPECTROSCOPY

VERENISE MARTINEZ LOPEZ

Being able to sustain quantum states for long periods of time in a laboratory setting can enable a new era of fast performing computing and secure communication. However, decoherence induced from low-energy defects limits quantum states to relatively short lifetimes and poses critical challenges for wide-scale application of quantum technology [1; 2; 3] . The core mechanism of this challenge has to do with noise induced from two-level tunneling states (TLS) at low-cryogenic temperature. The dissipation and noise is induced by interactions between TLS's and phonons found in amorphous materials. Recent theories show that TLS dynamics can be radically altered in reduced dimensional structures such as waveguides, nano electro-mechanical systems (NEMS), or nano resonators [4; 5; 6; 7; 8]. In our studies we conduct detailed noise measurements arising from TLS phonon dissipation via Brillouin spectroscopy. By looking at phonon dissipation rates at various cryogenic temperatures and comparing their trend with the expected TLS phonon attenuation rate we uncover the temperature scaling laws for dissipative and dispersive shifts in frequency in optical fibers. Our results show expected temperature dependence in TLS acoustic attenuation in a UHNA7 fiber and form the building blocks for uncovering the impact phonon confinement has on TLS physics.

ACKNOWLEDGMENTS

I would like to thank my research advisor, Ryan Behunin, for his constant support and dedication to my growth as a scientist. Thank you for sharing all your knowledge and wisdom to our group!

I would like to thank my committee members Angel Martinez and Christopher Mann.

I would like to thank Joel Johnson for being the best lab partner and motivating me through the long hours of lab work.

I would like to thank my mom, Elizabeth Martinez, for always encouraging me to pursue higher education and constantly believing in my strength. Esto es para ti.

Contents

1 Introduction **1**

1.1 Overview 1

2 Two-level Tunneling Theory **4**

2.1 Two-Level States 7

2.2 Acoustic Dynamics 9

2.3 Resonant and Relaxation Absorption 12

2.4 TLS in confined systems 15

3 Brillouin Scattering **18**

3.1 Stimulated Brillouin scattering 19

3.2 Electrostriction 21

3.3 Phase Matching Conditions 26

4 Methods **29**

4.1 AC Balanced Photodetection 30

4.2 Coherent Anti-Stokes Brillouin Scattering 34

5 Results **37**

6 Conclusion **47**

A Supplement Figures **48**

List of Figures

1.1 TLS lattice representation 2

2.1 Heat capacity for vitreous silica and crystalline quartz as a function of temperature 5

2.2 TLS Double Well Potential 7

3.1 Stimulated Brillouin scattering illustration 20

3.2 Dispersion relations for SBS 27

4.1 AC Balanced Photodetection 31

4.2 Probe power amplification 32

4.3 Power Transfer Spectrum 33

4.4 CABS Setup. 35

5.1 Illustration of optical fibers used in study 37

5.2 Power spectra of photonic crystal fiber taken at room temperature . 38

5.3 Power spectra of tapered fiber taken at room temperature 38

5.4 Power Spectrum measurement for UHNA7 at 800mK 40

5.5 Power spectrum for UHNA7 at 1.2K for 10mW and 30mW optical powers 41

5.6 Power transfer fit for incident powers between 10-90mW at 1.2K . . . 42

5.7 Power transfer fit for UHNA7 at 1-7K 43

5.8 Power transfer fit for UHNA7 at 5-9K 44

5.9 Linewidth vs Temperature measurements for UHNA7 at 5-9K 45

A.1 AC balanced photodetector circuit schematic 48

A.2 Intensity Modulator Diagram 49

A.3 Intensity Modulator voltage representation 49

Chapter 1

Introduction

1.1 Overview

The implementation of quantum mechanical properties into telecommunication and information science offers advantages such as the inability to clone quantum information, large computational space, and extensive encoding protocols for information transfer [9]. Though the use of quantum information science (QIS) shows a huge promise in advancing our information processing capabilities, the implementation of QIS is limited by short quantum state lifetimes. Many engineers have tried to combat this problem by introducing quantum systems into low cryogenic temperatures so as to reduce thermal fluctuations. However, at low enough temperatures an additive source of noise has been proven to arise from low-energy defects in a variety of disordered materials that hinders these quantum states [3; 10; 11]. These defects are theoretically described by the two-level tunneling state model, where it is said that there exists atoms or groups of atoms that can tunnel between two potential minima [12]. An illustration of this property is shown in figure 1.1. The ability to describe TLS's as atoms that can tunnel between two local minima bring about unique coupling dynamics with vibrational modes (phonons) and microwaves present in the

disordered material. These coupling dynamics give rise to phonon/photon dissipation that induce noise into their environment, thus they are one of the main drivers for quantum state decoherence. In order to benefit from quantum properties it is essential to understand both thermal and mechanical dynamics of TLS's.

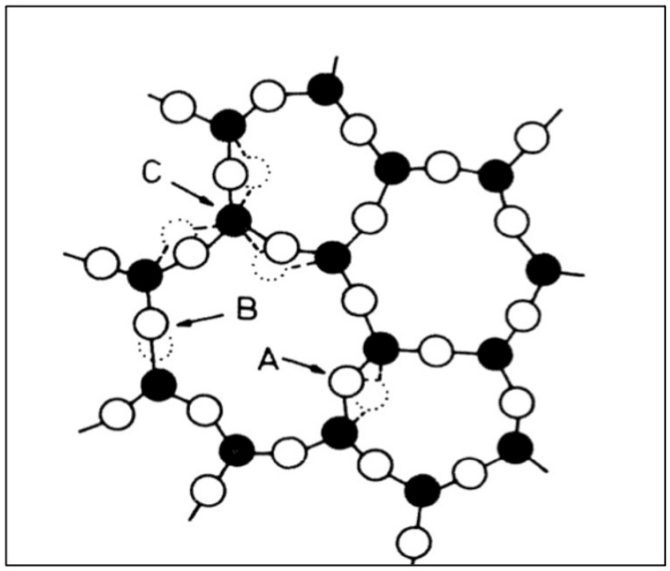

Figure 1.1: A schematic of a disordered lattice structure, where black and white circles represent different element atoms. Arrows for C, B, and A represent theoretical interpretation of two-level tunneling states [13].

In addition, the increase of nanoscale electronics such as nano-electro-mechanical systems (NEMS), highly confined photonics, and nano/micro mechanical resonators has caused a high demand in understanding how TLS's act in confined systems. Detailed work from [7] has shown that the dimensional reduction of opto-mechanical systems gives rise to new forms of TLS induced noise that are dependent on geometrical phonon confinement, TLS concentrations, and temperature. In reference [7] proposes that this dimensional dependence of TLS induced noise can offer methods to alter and control TLS-phonon noise. This was shown in reference [8], where it was found that TLS induced damping in nanomechanical resonators was restricted to the dimensions of their devices. These findings prompted our team to undertake the task

of developing a method for studying and measuring TLS dynamics in mechanically confined systems in order to expand the knowledge of low-energy defect noise and uncover optimal geometries for nano-structured devices.

We propose to study TLS-phonon dynamics via stimulated brillouin scattering (SBS) due to its coherent acousto-optic coupling, its ability to determine elastic properties of materials, its precision spectroscopy, and its coupling enhancement in confined systems [14; 15; 16; 17; 18]. In this work we investigate the phonon dissipation due to TLS-phonon coupling in optical fibers as a testing-ground for understanding how confined systems alter TLS dynamics and discern the accuracy of the TLS model in representing acoustic attenuation as shown in reference [7; 19]. Our work demonstrates the implementation of backwards SBS in a ultra-high-numerical-aperture (UHNA7) optical fiber, a photonic crystal fiber, and a tapered fiber in order to measure the phonon dissipation rates at cryogenic temperatures. We find that the phonon dissipation in UHNA7 can be modeled using TLS relaxation absorption and an offset that describes any background acoustic attenuation. Our studies contribute to the ongoing experimental work in trying to uncover TLS behavior in opto-mechanical systems and are the first ever evidence of TLS induced dissipation in an optical fiber at Northern Arizona University.

In chapters 2 we will go over the general understanding of the TLS model, its acoustic dynamics, and a treatment of TLS dynamics in confined systems as described by W.A. Phillips, S. Hunklinger, M.Schickfus, and R. Behunin, respectively [7; 12; 13]. Following the TLS model, chapters 3 and 4 will describe the mechanism of stimulated brillouin scattering and the two techniques used to conduct phonon spectroscopy using backwards SBS. Finally, in chapter 5 we will go over the phonon dissipation measurements taken at laser powers between 1mW - 90mW and at cryogenic temperatures between 800mK-9K. We conclude this study with implications of our results and continuing directions for this study.

Chapter 2

Two-level Tunneling Theory

The two-level tunneling state model formed the framework for describing thermal properties of amorphous material at low cryogenic temperatures around the 1970's when physicists R.C. Zeller and R.O. Pohl first studied the thermal properties of various "glassy" material at temperatures below 10K and compared them to crystalline material [20]. In their study it was shown that the thermal conductivity and heat capacity for multiple vitreous glass contrasted that of crystalline material, such that the heat capacity of vitreous glass increased linearly at temperature below 10K and the heat capacity of a crystalline quartz followed the critical specific heat as described in the Debye model. This is shown in figure 2.1. This was a monumental discovery since solid-state physics argued that thermal behavior of materials at low-cryogenic temperatures should not be affected by the materials structure given that at these temperatures materials are governed by long phonon wavelengths that are insensitive at the microscopic level. Thus, it was expected that the total amount of energy needed to cause any thermal increase should be the same for glasses and crystals. This discrepancy raised questions on whether the nature of disordered structures in materials gave rise to new thermal behaviors at the microscopic level.

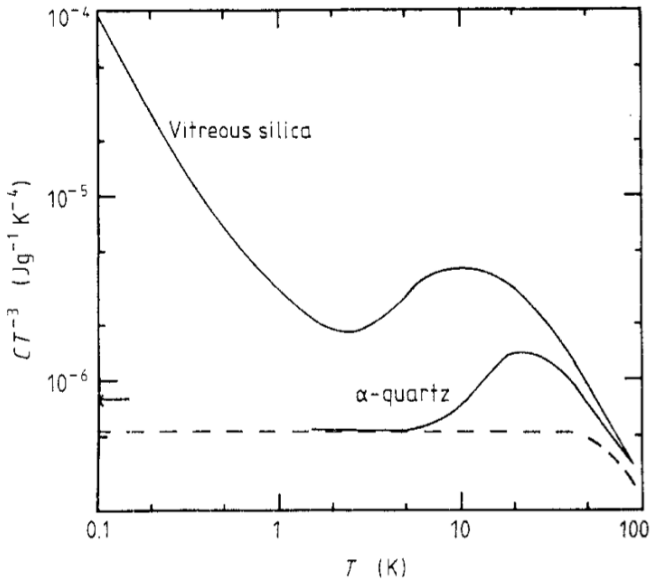

Figure 2.1: Heat capacity $C(T)/T^3$ for vitreous silica and crystalline quartz as a function of temperature between 0.1K - 100K [20].

It was the work of W. A. Philips, A.C. Anderson, B. Golding, and J. E. Graebner that proposed that the thermal discrepancies between glasses and crystals could be described by "atoms" or "group of atoms" that could quantum mechanically tunnel between two potential well minima. This model is what we now know of as the two-level tunneling state (TLS) model. By using quantum mechanics and the Wentzel-Kramers-Brillouin (WKB) approximation, they were able to treat these "atoms" as two-level states whose potential minima represented two discrete energy states. Thus, by accounting for these low-energy TLS's they were able to theoretically describe the linear temperature dependence of glasses heat capacity at low cryogenic temperatures and find similar temperature scaling laws for the conductivity of several glasses and crystals [12]. Given that we can treat TLS's as "atoms", it has been found that TLS's couple with phonons and microwaves present in their environment, with TLS-phonon coupling being the dominant source of TLS dynamics.

Though the TLS model accurately describes most of the thermal behaviors of glasses at low cryogenic temperatures much of this work is only capable of describ-

ing these dynamics at the macroscopic level. This left a gap between our knowledge of TLS behavior at the microscopic level and whether TLS-TLS interactions posed an impact on the proposed thermal behavior of disordered materials. Evidence of this lack of knowledge is emphasized by the measurements of the TLS density of states (DoS) in various glasses since it has been shown that TLS's scatter phonons at relatively similar rates for all glasses [21]. This is introduced in the TLS model via acoustic attenuation, which is composed of various material dependent numerical constants. These values consist of the coupling strength between TLS and local strains, the TLS density of states, the materials mass density, and the speed of sound. In reference [22], Y. Fu discusses how even though these values vary between glasses, when combined they give back a similar value for all glasses. He emphasizes that this universality could be better understood when taking into account TLS-TLS interactions. Most importantly, studying how TLS-TLS coupling scales in various systems such as optical fibers can give us insight of the microscopic TLS theory.

In the consecutive sections we will go over the basic theoretical framework of these two-level tunneling staet systems and their acoustic dynamics as described in [23] and [13]. In sections 2.3 and 2.4 we describe the markers of TLS-phonon coupling and the recent theoretical framework of these dynamics in confined systems. By examining how phonon dissipation changes at low cryogenic temperatures in optical fibers and comparing their trend with the theoretical TLS acoustic dynamics shown in sections 2.2 and 2.3, we were capable of developing a method for understanding quantum mechanical properties of materials in my laboratory setting.

2.1 Two-Level States

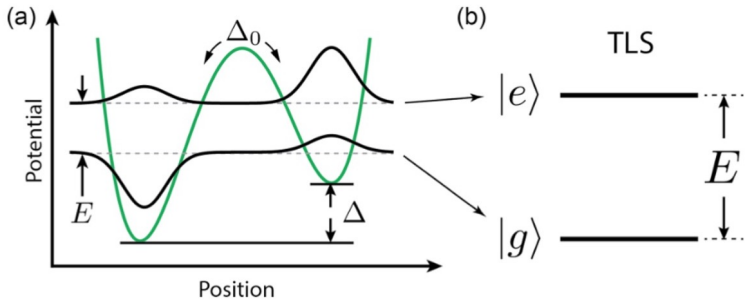

Figure 2.2: (a) Illustration of TLS double well potential with asymmetry Δ and tunneling strength Δ_o (b) Excited and ground eigenstate illustration of TLS with energy difference of E [7].

Two-level tunneling states were devised to resolve anomalous thermal properties of amorphous materials at low cryogenic temperatures, which could otherwise not be described using solid-state physics. At energy levels such that $k_B T \ll \hbar\omega$ a two-level state can be described through quantum mechanics via the Hamiltonian H_{TLS}.

$$H_{TLS} = \frac{1}{2}\begin{pmatrix} E_1 + \langle\phi_1|V - V_1|\phi_1\rangle & \langle\phi_1|H|\phi_2\rangle \\ \langle\phi_2|H|\phi_1\rangle & E_2 + \langle\phi_2|V - V_2|\phi_2\rangle \end{pmatrix}. \tag{2.1}$$

This is the localized representation of a TLS, where E_1 and E_2 are the TLS two ground state energies, V_1 and V_2 are the two harmonic-oscillatory potentials, and ϕ_1 and ϕ_2 are the two localised basis state representations. Here, each potential well can be considered as energy levels that can be associated with a difference from the TLS's zero energy level. An illustration of the TLS double potential well minima is shown in figure 2.2 [7]. If we assume our mean energy E_i is larger compared to $\langle\phi_1|V - V_i|\phi_1\rangle$ and we describe our zero energy as the mean energy of our two ground state energies

(E_i), we can then rewrite equation (2.1) as :

$$\frac{1}{2}\begin{pmatrix} -\Delta & \Delta_o \\ \Delta_0 & +\Delta \end{pmatrix} \quad , \tag{2.2}$$

where Δ is the relative energy difference described by the asymmetry of the potential wells and Δ_o is the tunneling strength between the two potential wells. Here Δ_o can be written as:

$$\Delta_o = 2\langle\phi_1|H|\phi_2\rangle = \hbar\Omega e^{-\lambda} \quad ; \quad \lambda = -d\left(\frac{2mV_o}{\hbar^2}\right)^{\frac{1}{2}} \quad , \tag{2.3}$$

where H is the complete TLS Hamiltonian $H = H_i - (V - V_i)$, Ω is the frequency of our TLS, m is the particles mass, V_o is the potential barrier between the two wells, and d it the separation between the two wells. The value λ corresponds to the tunneling strength that contributes to the system's thermal properties at a given temperature. We can diagonalize our Hamiltonian using the Pauli operators shown in equation (2.4) to obtain our energy eigenfunction : $H = \frac{1}{2}E\sigma_z$, where $E^2 = (\Delta^2 + \Delta_o^2)^{\frac{1}{2}}$.

$$\sigma_x = \begin{pmatrix} 0 & 1 \\ 1 & 0 \end{pmatrix}, \quad \sigma_y = \begin{pmatrix} 0 & -i \\ i & 0 \end{pmatrix}, \quad \sigma_z = \begin{pmatrix} 1 & 0 \\ 0 & -1 \end{pmatrix}. \tag{2.4}$$

It has been theoretically shown that there is a correlation between Δ and Δ_o that comes from contribution of neighboring TLS interactions. These TLS-TLS interactions affect the barrier height and asymmetry for our double well potential system [24]. However, in our experiments we treat our potential wells separated at a distance comparable to the distance of atoms in solids. Taking on this assumption, we evaluate a distribution function of the possible tunneling strengths (λ) and potential asymmetry (Δ) as $f(\Delta)d\Delta$. Here we treat $f(\Delta)d\Delta$ as a constant that is purely dependent on a fixed TLS density of states and a zero-point energy for symmetric potential wells

(Δ_o). This approximation gives us back : $f(\Delta)d\Delta = \frac{P}{\Delta_o}$. Where P corresponds to a constant TLS density of states. From this note, we will be able to move forward in describing a TLS interaction Hamiltonian capable of describing the consequences of TLS-phonon coupling.

2.2 Acoustic Dynamics

TLS's are subjected to interactions with varying strain fields that can be represented as acoustic fields (phonon modes). These interactions induce dipole moments that change the asymmetry energy and barrier height of the TLS that then influence absorption and emission of energy into their environment. In this section, we assess the coupling of TLS's with strain fields in the form of acoustic fields and/or electromagnetic fields. We begin by deriving the equations of motion for these interaction by writing a Hamiltonian representation of these elastic strain fields :

$$H = H_o + H_a = \frac{1}{2}\begin{pmatrix} E & 0 \\ 0 & -E \end{pmatrix} - \begin{pmatrix} D & 2M \\ 2M & -D \end{pmatrix} e \quad , \tag{2.5}$$

here E represents the energy splitting of the TLS, D is the deformational potential that describes the energy shift of the relaxing state perturbed by the strain field e, and M is the deformational potential for transverse and/or transverse phonon modes. The first term, H_o, corresponds to the TLS without perturbations and H_a the interaction with elastic strain fields. This representation of the TLS-interactions allows for an interchangeable formulation of TLS-phonon interactions or TLS-microwave interactions. Thus, we can also write H_a with respect to its dielectric properties when

coupling with electromagnetic fields :

$$H_e = \frac{1}{2}\begin{pmatrix} \mu & \mu' \\ \mu' & -\mu \end{pmatrix} F(t), \tag{2.6}$$

where μ and μ' correspond to the permanent and induced dipole moment, respectively. The function $F(t)$ is introduced to represent the interaction of the systems with a time-varying electric field. Using Golding and Graebner's formalism we can connect both Hamiltonian interpretations and derive equations of motion that are analogous to a spin $\frac{1}{2}$ systems that describes the nuclear magnetic resonance. This is given by reference [25] :

$$\begin{aligned} \dot{X} &= \frac{-X}{T_2} - (E + De)\frac{Y}{\hbar} \quad , \\ \dot{Y} &= (E + De)\,\frac{X}{\hbar} - \frac{Y}{T_2} - \frac{2Me}{\hbar}Z \quad , \\ \dot{Z} &= \frac{2Me}{\hbar}Y - \frac{(Z - Z_e)}{T_1} \end{aligned} \tag{2.7}$$

where T_1 and T_2 are the TLS decay rate and dephasing rate, respectively. X and Y are the elastic and electric induced polarization, respectively. Z corresponds directly to the systems polarization. In the $\dot{Z}$ expression, Z_e corresponds the polarization at instantaneous equilibrium :

$$Z_e = \frac{1}{2}\tanh\left[\frac{(E + De)}{2k_B T}\right] \tag{2.8}$$

If we take a first order approximation of $\dot{Z}$ we can rewrite Z_e as the population difference at thermal equilibrium and the change in the population as the energy deviates :

$$Z_e = Z_o + De\frac{dZ_o}{dE} \quad ; \quad Z_o = -\frac{1}{2}\tanh\left(\frac{E}{2k_B T}\right). \tag{2.9}$$

Rewriting Z this way gives us a description of the TLS energy attenuation produced by a relaxation process from TLS-strain field interactions.

Now that we have a set of equations that can describe the acoustic dynamics of TLS-phonon interactions, we can take on the case where we have time-varying strain fields : $e = e_o \cos \omega t$. Since we have time dependent strain fields it is necessary to take into account their pulse duration (τ_p). We can then categorize two cases where $\tau \ll T_1, T_2$ or $\tau \ggg T_1, T_2$. In our experiments, we are working with CW incident fields, so we take on the first case when continuing the description of TLS-phonon dynamics. When working in this regime, we can say that all short-lived exponential's will decay prior to the end of our applied field. This allows us to solve for an induced elastic field polarization given by :

$$\dot{X} = \frac{Me}{\hbar}\left(Z_o + \overline{Z}\right)\left[\frac{1}{(\omega_o - \omega) - i(T_2)^{-1}} + \frac{1}{(\omega_o - \omega) + i(T_2)^{-1}}\right] \quad , \tag{2.10}$$

where ω_o is the TLS resonance frequency, ω is the frequency of our oscillatory field, and T_2 is the TLS dephasing rate. In addition $\overline{Z}$ is time independent and defined as:

$$\overline{Z} = \frac{-M^2 e_o^2 T_1 T_2 \frac{Z_o}{\hbar^2}}{1 + (\omega_o - w)^2 T_2^2 + M^2 e_o^2 T_1 T_2 \frac{Z_o}{\hbar^2}} \quad , \tag{2.11}$$

Using the $\overline{Z}$ expression you can find an approximate value for the amplitude for Z-component polarization given by :

$$\hat{Z} = -De\left(\frac{dZ_o}{dE}\right)\left(\frac{1 + i\omega T_1}{1 + \omega^2 T_1^2}\right). \tag{2.12}$$

In summary, we can correlate a TLS acoustic dynamics with a spin-$\frac{1}{2}$ system such that we can derived equations of motion for the TLS interaction Hamiltonian H using Bloch's equations. We take the appropriate approximations for our experimental set

up such that τ_p is selected to represent a "steady-state" solution for our oscillatory fields $e(t)$. In order to measure the influence TLS-phonon coupling has on a materials acoustic properties we calculate the internal energy of the amorphous material given by :

$$\delta U = -N(2Me, 0, De) \cdot (X, Y, Z) \quad , \tag{2.13}$$

where N is the number of TLS per unit volume. Using this energy definition we get back elastic modulus C as a function of the TLS equations of motion described in (2.7) :

$$\delta C = \frac{1}{e}\frac{\partial(\delta U)}{\partial e} = -\frac{N}{e}(2MX + DZ) \tag{2.14}$$

The dependence of Z and X in equation (2.14) gives insight on the absorption properties of a TLS-phonon interaction. These absorption properties are the key markers we use in our studies to interpret the level of acoustic attenuation coming from our active TLS's in our optical fibers. In the next sections we will talk about these dynamics and open up the conversation on how we study TLS dynamics in confined systems.

2.3 Resonant and Relaxation Absorption

To understand the acoustic attenuation induced by TLS's we begin by distinguishing the two contributions found in the equation (2.14), which correspond to unique acoustic absorption mechanisms. We find that X term in equation (2.14) leads to a resonant phonon absorption between coupling of TLS's and phonons with the same energy. This is governed by $\dot{X}$. The Z term in (2.14) leads to the modulation of the TLS'S two occupied states, which bring the TLS out of thermal equilibrium. This results in irreversible relaxation process where the TLS absorbs energy from a phonon and emits that energy into its environment. We evaluate this notion by plugging in

equation (2.7) into (2.14) and integrating over all energy splitting. This gives us back a resonant absorption value emanating from the imaginary part of elastic modulus:

$$\alpha_{res} = \frac{\pi n_a M^2 \omega}{\rho v^3} \left(\frac{\tanh\left(\frac{\hbar\omega}{2k_B T}\right)}{\sqrt{1+\frac{I}{I_c}}} \right) \quad ; \quad I_c = \frac{\hbar^2 \rho v^3}{2M^2 T_1 T_2} \quad , \tag{2.15}$$

where n_a is the TLS density of states, ω is the phonon resonance frequency, ρ is the volume mass density, v is the speed of sound, T is the temperature in the system, and I_c is the so called critical acoustic intensity. There are two important details to notice from equation (2.15). The first is that as I_c becomes larger I, resonant absorption begins to decrease. This indicates that phonon dissipation produced by resonant absorption can be saturated by probing the TLS with high acoustic intensities.

The second factor of equation (2.15) is that α_{res} has a hyperbolic tangent temperature dependence which indicates that as T decreases to very low cryogenic temperatures there is an increase in phonon dissipation originating from resonant absorption. This is due to the fact that at low enough temperatures there will be a high concentration of TLS's in their ground state, which will then allow for stimulated phonon absorption. In the case of high temperatures, most of TLS's can be found in their excited state so stimulated phonon emission dominates. As temperatures increase, both stimulated phonon emission and absorption compensate each other and resonant absorption is suppressed [19]. In essence there are three key regimes for resonant absorption: *i*) at low cryogenic temperatures you have an increase in resonant absorption *ii*) at high temperatures this process is compensated by stimulated phonon emission *iii*) at low temperatures but high acoustic intensities, TLS's who have absorbed a resonant phonon and are now in their excited state begin to be probed by a high concentration of phonons. This happens at a rate faster than the TLS's decay rate so the probing phonons induce stimulated phonon emission which leave the probed phonon unaltered.

Next, the second term of equation (2.14) can be associated a relaxation process. Relaxation absorption can be described as a modulation of the TLS energy splitting due to time-dependent strain fields, $e(t)$. In this process TLS's are driven out of thermal equilibrium, which cause TLS's to absorb energy from neighboring phonons in the process wanting to come back to thermal equilibrium. The TLS will then absorb energy from a phonon and release it into its environment in a irreversible manner. This modulation thus leads to the dissipation and frequency shift of phonons. Relaxation absorption can be described as :

$$\alpha_{rel} = \frac{k^3 T^3 \zeta(4, 0.5)}{32\pi\rho^2\hbar^4 v^3} n_a D^2 \left(\frac{M_l^2}{v_l^5} + \frac{2M_t^2}{v_t^5} \right) \quad , \tag{2.16}$$

here $\zeta(4, 0.5)$ corresponds to the Riemann zeta function. In addition, M_l and M_t represent our deformational potential with respect to longitudinal and transverse acoustic fields. Lastly, v_t and v_l are the speeds of these transverse or longitudinal phonon fields, respectively. The key markers that differentiate this absorption process from α_{res} is that α_{rel} has a cubed temperature power law. This indicates that as cryogenic temperatures increase, phonon dissipation is governed by relaxation absorption. In addition, the speed dependence of α_{rel} gives rise to temperature dependent variations of the speed of sound in the material. This speed variation is given by [12]:

$$v(T_o) - v(T) = \frac{P\gamma^2}{\rho v} \ln \frac{T}{T_o} \tag{2.17}$$

, when taking the approximation that $\Omega\hbar \lll k_B T$. T_o is set to the initial temperature in measuring relaxation absorption and T as the temperature difference from T_o.

In this project, the temperature dependence and acoustic intensities are used to differentiate whether our phonon dissipation measurements are capturing resonant or relaxation absorption originating from TLS-phonon interactions. The phonon dissipation rates are measured using stimulated brillouin scattering at various cryogenic

temperatures. The phonon dissipation is then plotted as a function of temperature and fit with either Γ_{res} or Γ_{rel} to see if we can describe the dissipation trend with TLS acoustic dynamics. Here Γ_{res} is given as $\Gamma_{res} = \alpha_{res} v$ and Γ_{rel} as $\Gamma_{rel} = \alpha_{rel} v$. In the continuing section, we describe how these dynamics are altered by selecting systems that showcase phonon confinement.

2.4 TLS in confined systems

Bulk amorphous materials with high concentrations of TLS's have been extensively studied in [26; 12; 13], where effects of geometrical confinement can be neglected. To this date, the TLS model has been able to describe the observed acoustic dynamics in bulk systems, however within highly confined optical and mechanical systems it has been found that it is no longer appropriate to use the TLS model [22; 27; 28]. This has to do with the fact that active TLS's are highly dependent on the phonon density of state in their environment. This means that as you alter the phonon mode structure of materials/devices there is a potential to alter the availability for resonant TLS-phonon coupling. In addition, not much is known about the behavior of TLS's in reduced dimension where TLS-TLS interactions are no longer negligible [22].

In recent theoretical work from [7], it was shown that TLS phonon dynamics and noise can be altered in systems such as resonators and waveguides. They hypothesized that the phonon dissipation from relaxation and resonant absorption changed as a function of their systems dimension. The dimensional dependence of TLS phonon absorption can be described using the phonon decay rate given by :

$$\Gamma_{res} = P_D\left(\hbar\Omega_q\right) A \tanh\frac{\hbar\omega}{2k_BT}\left(\frac{1}{\sqrt{1+\frac{I}{I_c}}}\right) \quad \text{and} \quad \Gamma_{rel} = P_D\left(k_BT\right) B\left(k_BT\right)^D \quad , \tag{2.18}$$

here we take a simplified version of equation (35) and (29) from reference [7], where

P_D is the TLS density of states dependent on the dimensions D and A is a constant that encompasses material properties such the phonon deformational potential for the i-th phonon, the speed of sound v, and mass density ρ. The constant B also encompasses material properties such as the speed of sound v, the mass density ρ, and the sum of the phonon deformational potential to the forth power over the speed of sound squared for the i-th phonon mode.

In recent work from [8], it was confirmed that the theoretical work shown in reference [7] accurately described the observed damping rate in 1-Dimensional and 2-Dimensional aluminum NEMS resonator devices. In reference [8], they measure the damping rate of four NEMS devices with "narrow" and "wide" dimension specifications (down to the micron level) and fit the trend with the dimensional dependant relaxation absorption function. They find that the temperature dependence in their damping rate Δf (MHz) follows the same trend at $\Gamma_{rel,1D}$ and $\Gamma_{rel,2D}$ for the "narrow" and "wider" devices, respectively. This confirmed that dissipation in their systems originated from TLS relaxation absorption at low cryogenic temperatures. In addition, in work presented from [5] they studied the damping of mechanical oscillations in a NEMS device that originated from TLS phonon dissipation. In doing so, they measure the inverse quality factor and fit their results with an inverse quality factor $Q^{\frac{1}{3}}$ for a one dimensional system as described in [7]. They find that they can describe the damping rate in the NEMS device via the 1-D inverse quality factor arising from relaxation absorption caused by excitation of TLS-flexural mode coupling.

In both of these studies, we can treat the phonons in each system as confined to one or two dimensions, which drastically alter the temperature dependence of the dissipation produced from TLS's. Experimental validity of the TLS model in confined system opens up new capabilities for improving the performance of a quantum devices. This can be done by embedding quantum systems inside confined mechanical structures (such as an acoustic resonator), where TLS dissipation and noise can

be altered and reduced, thus reducing the amount of noise introduced in the overall quantum device. Though this work is very promising for advancing applications of quantum devices, it is necessary to conduct preliminary experiments to test practical implementation of this work. The main inquiries are: *i*) to what extent can the TLS model for confined structures accurately describe the dissipation in its system and *ii*) could confined structures bring about systematic effects that alter the quantum device. In this study we propose to conduct preliminary experiments in optical fibers that showcase confinement and build a technique for measuring TLS dynamics in these systems.

Chapter 3

Brillouin Scattering

Light-matter interactions are one of the key dynamics for understanding the thermodynamic and mechanical properties of materials [29; 17]. One of the main scattering processes used in photonics is the coupling of light and vibrational modes in materials. The main scattering processes are known as Raman, Brillouin, and Rayleigh scattering. Raman and Brillouin scattering both occur from coupling between optical and acoustic fields in the material. However, Brillouin scattering occurs from light coupling to traveling acoustic waves and Raman scattering occurs from light coupling to standing compressional waves in material that originate from oscillations of atomic bonds. Acoustic waves in material can originate from thermal/quantum fluctuations or driven via external optical fields.

In the consecutive sections we will go over the basic theoretical framework for stimulated Brillouin scattering and phase matching conditions. We detail the implication of induced optical fluctuations in materials and how they give rise to stimulated Brillouin scattering as described in reference [29]. We exploit the energy transfer mechanisms in stimulated Brillouin scattering by measuring how the phonon decay rates change at cryogenic temperatures and for different acoustic field intensities. Thus, allowing for a quantitative analysis of TLS dynamics in opto-mechanical structures

such as optical fibers.

3.1 Stimulated Brillouin scattering

Brillouin scattering is a chi-3 nonlinearity that involves electrostriction and photoelasticity. Brillouin scattering can occur in two different ways: spontaneous or stimulated. Spontaneous Brillouin scattering occurs when light fields couple to vibrational modes that come from thermal fluctuations, usually through variations in the dielectric constant. On the other hand, you can have stimulated Brillouin scattering (SBS) from induced coherent vibrations in the material created from external optical fields. These vibrations are said to be stimulated via changes in the refractive index in material originating from the intensity of your applied field. In our study, we utilize backwards SBS given its higher scattering sensitivity of the order 10^5 compared to spontaneous [29] and its ability to transfer energy between two incident beams. In the present section we will go over the mechanisms of SBS followed by its phase matching conditions.

SBS occurs when an external incident field of frequency ω_p couples with the acoustic fields in the material of frequency Ω_B, which produce a backscatter of frequency ω_s. Since our incident field is propagating in the same direction as our acoustic field, the scattered light is downshifted to the Stokes frequency of the form : $\omega_s = \omega_p - \Omega_B$. The stimulated aspect of this process is that the interference frequency of the Stokes backscatter and the incident field will produce a response in the material that increases the amplitude of the acoustic field, usually produced by electrostriction. A diagram of the SBS process is shown in figure 3.1(a).

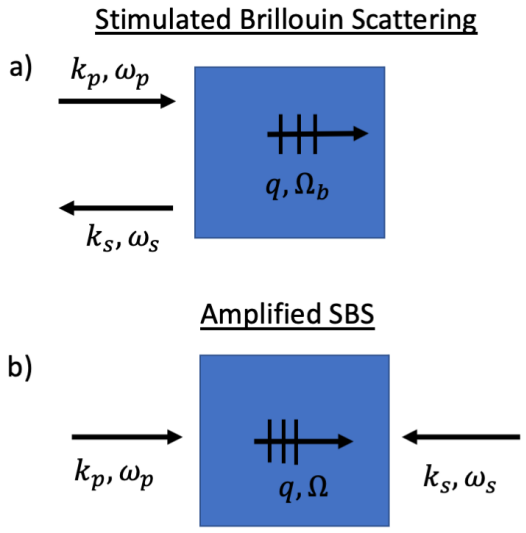

Figure 3.1: (a)Illustration of stimulated Brillouin scattering where k_p is our external optical field and k_s, q_B are internal fields that grow due to high light-matter interaction regions (b) Illustration of stimulated Brillouin scattering when two external fields (k_p, k_s) produce a beat-note at a frequency and wave-vector difference between both applied fields.

This process can be studied in two manners: generated and amplified SBS. Generated SBS happens when the Stokes field and acoustic field do not originate externally. In generated SBS one incident field originates from a high intensity beat tone from the phonons inherent to your material and the other incident field is external. Amplified SBS occurs when two counter-propagating external fields interact with the material such that they create a beat-note (sound wave). Generated and amplified SBS is shown in figure3.1(a) and 3.1(b), respectively.

In our study we utilize amplified SBS, where both our incident beams are introduced to the sample externally. Here the pump and Stokes external fields produce a beat note that amplifies the acoustic fields in the sample by producing a dense region of high optical intensity(electrostriction) and in return the amplified acoustic field drives a Doppler shift that induces a transfer of energy from the pump to Stokes at the resonance frequency Ω_B(photoelasticity). Moving forward, we will give a detailed

description of electrostriction using the notation from reference [29] and explain how we propose to use SBS for our TLS analysis.

3.2 Electrostriction

Stimulated Brillouin scattering (SBS) is a coupling mechanism that occurs from an optical response induced from electrostrictive forces. In the global aspect, electrostrictive forces are a consequence of energy storage that originates from changes in the potential energy per unit volume as you apply external fields. Microscopically, electrostrictive forces act on the molecular structure of the material, which then develop a dipole moment of : $\mathbf{p} = \epsilon_o \alpha \mathbf{E}$. Here ϵ_o is the permittivity of free space and α is the molecular polarization. We can represent these forces thus as a change in energy in the presence of an electric field:

$$\mathbf{F} = -\nabla U = \frac{1}{2}\epsilon_o \alpha \nabla (E^2). \tag{3.1}$$

A consequence of the electrostrictive forces, $\mathbf{F}$, is that molecules pulled from these forces create an increase in material density at a given region. The change of density in the material then produces a rippling effect that in turn induces a change in the dielectric constant $\epsilon + \Delta\epsilon$. This tell us then that the change in energy per unit volume Δu is associated to the change in dielectric complemented with a change in density:

$$\Delta u = \frac{1}{2}\epsilon_o E^2 \Delta\epsilon = \frac{1}{2}\epsilon_o E^2 \left(\frac{\partial \epsilon}{\partial \rho}\right) \Delta\rho \quad , \tag{3.2}$$

here Δu is associated with the work used to constrict the material, Δw. Where Δw is proportional to the change in the materials density and a restrictive pressure (p_r) in the presence of an electric field. The expression for Δw can then be written as : $\Delta w = -p_r \frac{\Delta\rho}{\rho}$. By equating Δu with Δw, we find that the electrostrictive pressure is

given as:

$$p_r = \frac{1}{2}\epsilon_o E^2 \left(\frac{\partial \epsilon}{\partial \rho}\right) \rho = \frac{1}{2}\epsilon_o \gamma_e E^2 \quad , \tag{3.3}$$

here γ_e can be estimated using the Lorentz-Lorenz law that predicts the electrostrictive constant as a function of the nonlinear refractive index coefficients : $\gamma_e = \frac{(n^2-1)(n^2+2)}{3}$. Now that we have the electrostrictive pressure identified with respect to the electric field, we can calculate the change in density with respect to p_r. More specifically, we can associate the change in material density with the an applied electric field:

$$\Delta\rho = -\rho C p_r = \frac{1}{2}\epsilon_o C \gamma_e \langle \tilde{\mathbf{E}} \cdot \tilde{\mathbf{E}} \rangle. \tag{3.4}$$

In equation (3.4), the parameter C corresponds to the compressibility $C = \rho^{-1}\left(\frac{\partial \rho}{\partial p}\right)$. The angular brackets indicate the time average over the optical period. From here we can evaluate the changes in optical properties due to electrostriction. We focus on the change in susceptibility since it corresponds to a change in the materials properties as a result of light. Here the change in susceptibility $\Delta\chi$ corresponds to the change in the dielectric constant $\Delta\epsilon$. Using relationship in equations 3.2 and equation 3.4 we get back the susceptibility as a function of the electric field:

$$\Delta\chi = \frac{1}{2}\epsilon_o C \gamma_e^2 \langle \tilde{\mathbf{E}} \cdot \tilde{\mathbf{E}} \rangle. \tag{3.5}$$

Thus, associating susceptibility of a material by the compressive strength, our applied optical field, and the electrostrictive constant squared.

In our studies, we focus on electric fields that contain more than one frequency component such that we have to evaluate C and γ_e at constant entropy to determine the response of the $\tilde{E}$ field. Taking on this case, we represent $\tilde{E}$ as a configuration of

our Stokes back scattered field and pump field:

$$\begin{aligned} \tilde{E} &= \tilde{E}_s\left(z,t\right) + \tilde{E}_p\left(z,t\right) \quad , \\ \tilde{E}_p\left(z,t\right) &= A_s(z,t)e^{i(k_p z-\omega_p t)} + c.c \quad , \\ \tilde{E}_s\left(z,t\right) &= A_p(z,t)e^{i(-k_s z-\omega_s t)} + c.c \end{aligned} \tag{3.6}$$

We then represent the acoustic fields in terms of the material density distribution :

$$\tilde{\rho}(z,t) = \rho_o + \rho(z,t)e^{i(qz-\Omega t)} + c.c \tag{3.7}$$

It is important to note that Ω here corresponds to the frequency in which you drive the beat note in the material, which is not the same as the brillouin frequency, Ω_B. This will be spoken in detail in the next section. In addition, $E_s\left(z,t\right)$ corresponds to the Stokes incident field and $E_p\left(z,t\right)$ is with respect to the pump counter propagating field. Next, we introduce our acoustic field into the wave equation:

$$\frac{\partial^2\tilde{\rho}}{\partial t^2} - \Gamma'\nabla^2\frac{\partial\tilde{\rho}}{\partial t} - v^2\nabla^2\Delta\tilde{\rho} = -\nabla\cdot\mathbf{f} \quad , \tag{3.8}$$

here v is the speed of sound and Γ' is the damping parameter written as $\frac{\Gamma}{q^2}$. The right side of equation (3.8) corresponds to the divergence of the force per unit volume, where $\mathbf{f} = \nabla p_r$. By substituting our $\mathbf{f}$ with equation (3.8) and $\tilde{E}$ with equation (3.6) we get back :

$$\nabla\cdot\mathbf{f} = \epsilon_o\gamma_e q^2\left[A_p A_s^* e^{i(qz-\Omega t)} + cc\right]. \tag{3.9}$$

Since $\tilde{E}_s$ is counter propagating with respect to the acoustic and pump fields, $\nabla\cdot\mathbf{f}$ is associated to a wave field with a frequency equal to the difference between the Stokes and pump electric fields : $\Omega = \omega_p - \omega_s$ and its wave-vector component as : $q = k_p - k_s$. Now we can introduce our equation (3.9) and (3.7) into the full wave equation again. After taking time derivatives, the Laplacian of our acoustic wave field, and assuming

the slowly-varying amplitude approximation for our acoustic field we get back:

$$\epsilon_o \gamma_e q^2 A_s A p^* = -2i\Omega \frac{\partial \rho}{\partial t} + (\Omega_B^2 - \Omega^2 - i\Omega\Gamma_B)\rho - 2iqv^2 \frac{\partial \rho}{\partial z} \quad , \tag{3.10}$$

here the Brillouin linewidth is added to associate the frequency shift of the SBS process to the phonon decay rate and the magnitude of the wave-vector : $\Gamma_B = \Gamma' q^2$. The phonon-lifetime is the reciprocal of the Brillouin linewidth $\tau = (\Gamma_B)^{-1}$. We can take this further and understand how the spatial evolution of our optical fields vary with respect to their wave amplitudes and the material properties such as χ, Γ_e, and ρ. We describe the spatial evolution of the optical field through the wave equation:

$$\frac{\partial^2 \tilde{E}_i}{\partial z^2} - \frac{1}{(\frac{c}{n})^2} \frac{\partial^2 \tilde{E}_i}{\partial t^2} = \frac{1}{c^2 \epsilon_o} \frac{\partial^2 \tilde{P}_i}{\partial t^2}. \tag{3.11}$$

We can then substitute $\tilde{E}_i$ with our $E_p(z,t)$ and $E_s(z,t)$, respectively. We can then represent the nonlinear polarization, $\tilde{P}_i$, with respect to the electrostrictive constant and the materials density by : $\tilde{P}_i = \epsilon_o \Delta\chi \tilde{E}_i = \epsilon_o \rho o^{-1} \gamma_e \tilde{\rho} \tilde{E}$. Putting $\tilde{P}_i$ and $\tilde{E}_i$ into equation (3.11) and taking the slow-varying amplitude approximation you get back the wave equations for each optical field as:

$$\begin{aligned} \frac{\partial A_p}{\partial z} - \left(\frac{1}{\frac{c}{n}}\right) \frac{\partial A_p}{\partial t} &= \frac{i\omega\Gamma_e \rho A_s}{2nc\rho_o} \quad , \\ \frac{\partial A_s}{\partial z} - \left(\frac{1}{\frac{c}{n}}\right) \frac{\partial A_s}{\partial t} &= \frac{i\omega\Gamma_e \rho^* A_p}{2nc\rho_o} \quad , \end{aligned} \tag{3.12}$$

here ρ is the steady state solution for equation (3.8), when effects of v are ignored. In addition, by taking on a steady state condition we can drop the spatial derivatives found in (3.10) and describe the acoustic amplitude as :

$$\rho(z,t) = \epsilon_o \Gamma_e q^2 \frac{A_p A_s^*}{\Omega_B^2 - \Omega^2 - i\Omega\gamma_B}. \tag{3.13}$$

The importance of identifying the wave equations of the two propagating optical fields as a function of their amplitudes is so we can introduce the intensities of two interacting optical fields. This gives us:

$$\frac{dI_p}{dz} = \frac{dI_s}{dz} = -g_B I_p I_s \quad , \tag{3.14}$$

$$g_B = g_o \frac{(\frac{\Gamma_B}{2})^2}{(\Omega_B - \Omega)^2 + (\frac{\Gamma_B}{2})^2} \quad ; \quad g_o = \frac{\gamma_e \omega^2}{nvc^3 \rho_o \Gamma_B} \quad , \tag{3.15}$$

here the change in intensity is driven by the SBS gain factor g_B, which is inversely proportional to the phonon decay rate, the phonon resonance frequency Ω_B, and the acoustic amplification frequency Ω. The result shown in equations (3.15) allude to a transfer of power between the two incident optical fields pump and Stokes such that we can write the SBS gain factor in terms of the power of our optical fields. This is written as:

$$\Delta P = G_b P_p P_s L \frac{(\frac{\Gamma_B}{2})^2}{(\Omega_B - \Omega)^2 + (\frac{\Gamma_B}{2})^2} \quad , \tag{3.16}$$

here G_B is the Brillouin gain coefficient, P_p is the pump power, P_s is the Stokes power, and L is the length of the material sample. It is important to note that amplified SBS is a resonant process that requires that all optical fields be phased matched with the acoustic fields in material. In the next section, we will go over the phase-matching conditions required to induce amplified SBS.

The essential part of the amplified SBS process is that we retrieve the Brillouin gain, speed of sound, and phonon decay rate by measuring the power amplification, ΔP. This relationship is used in our studies where we induce amplified SBS and collect the Stokes signal after the wave amplification. We then use two methods: balanced photodetection and Coherent Stokes Brillouin Scattering(CABS) to measure ΔP. We propose to use SBS as a way to analyze the phonon dissipation induced via TLS-phonon coupling by measuring ΔP at various cryogenic temperatures and

comparing the linewidth (Γ_B) trend as a function of temperature with Γ_{res} or Γ_{rel}.

3.3 Phase Matching Conditions

In the previous section we learned that interference between two optical fields produces time-varying and spatially dependent optical forces that drive acoustic amplifications in materials [29]. The direction in which we propagate these optical fields can take the form of Forward SBS or Backwards SBS [15]. In our study we counter-propagate two external incident fields (pump/Stokes) into an optical fiber, which induces a Backwards SBS. Though SBS is a resonant process, there can still be scattering at various external field frequencies. This is illustrated in figure 4.3, where we have the power spectrum of the power transfer between pump and Stokes intensities. In this figure we get back the Brillouin linewidth, the phonon speed, and the brillouin gain. However, in order to have optimal power amplification it is necessary that the frequency interference between the Stokes and pump fields amount to the phonon resonance frequency, Ω_B. This process can be well understood through conservation of energy and momentum, which is usually regarded as phase-matching conditions.

We can describe the initial energy of the system as $E_{in} = \hbar\omega_p - \hbar\omega_s$ and the final energy equal to $E_{out} = \hbar\Omega_B$. We can also write the momentum equations for the initial and final state of our scattering process as $P_{in} = \hbar\mathbf{k}_p - \hbar\mathbf{k}_s$ and $P_{out} = \hbar\mathbf{q}_B$. Here Ω_B is the phonon resonance frequency and ω_p,ω_s represent the pump frequency and Stokes backscatter frequency, respectively. What makes Brillouin scattering a stimulated process is that the difference between the two counter propagating optical fields denotes the beat tone in which you amplify acoustic waves(phonons). Writing the phase-matching condition for amplified SBS take the form of:

$$\begin{aligned} \mathbf{q} &= \mathbf{k}_p - \mathbf{k}_s \quad , \\ \Omega &= \omega_p - \omega_s \quad , \end{aligned} \tag{3.17}$$

here Ω corresponds to the frequency in which the pump and Stokes fields drive the acoustic waves. We can find the phonon frequency by using the phase-matching condition for our pump, Stokes backscatter, and phonon dispersion relations. Since the pump field is propagating in the same direction as the acoustic field, the phase-matching conditions are given as :

$$\begin{aligned} \omega_s &= \omega_p - \Omega_B \quad , \\ \mathbf{k}_s &= \mathbf{k}_p - \mathbf{q}_B \quad , \end{aligned} \tag{3.18}$$

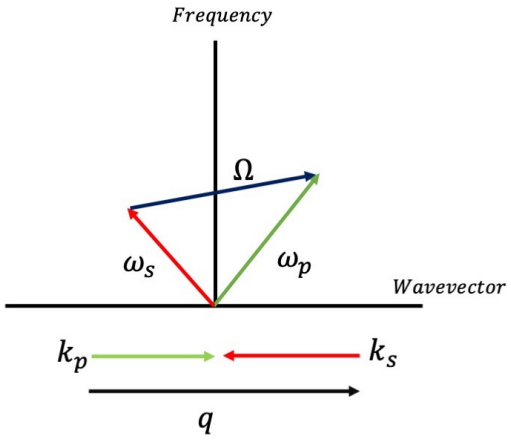

Figure 3.2: Dispersion relations for brillouin scattering shown in vector notation. Co-propagating pump and phonon field induces a lower frequency shift that results in a Stokes backscatter. Thus, the forward moving phonon connects the initial pump state to the final Stokes state

We can relate phonon wave-vector $\mathbf{q}_B$ to the phonon frequency by using the phonon and photon dispersion relationship : $|\mathbf{q}_B| = \frac{\Omega_B}{v_s}$ and $|\mathbf{k}_i| = \frac{n\omega_i}{c}, i = p, s.$ By applying these dispersion relations into equation (3.18) and using the fact that our Stokes field is propagating in the opposite direction from the pump and acoustic

fields we get back:

$$\begin{aligned} \Omega_B &= v_s \left(\frac{n\omega_p}{c} - \left(-\frac{n\omega_s}{c} \right) \right) \quad , \\ \Omega_B &= \frac{v_s n}{c} \left(\omega_p + \omega_s \right) \quad , \end{aligned} \tag{3.19}$$

here v_s corresponds to the speed of sound, c is the speed of light, and n is the materials effective index of refraction. We can now use equation (3.17) to rewrite the optical frequency difference in equation (3.19) and eliminate the Stokes frequency dependence. This gives us:

$$\begin{aligned} \Omega_B &= \frac{\frac{v_s n}{c} 2\omega_p}{1 + \frac{v_s n}{c}} \quad , \\ \Omega_B &\approx \frac{2 v_s n}{c} \omega_p \quad , \end{aligned} \tag{3.20}$$

The second equation in (3.20) is derived by assuming that the nv_s is much smaller than c so we can approximate the denominator to be solely composed of c. Taking on this approximation, we can substitute equation (3.20) into the phonon dispersion relationship and get back the phonon wave-vector as a function of the pump wave-vector : $\mathbf{q}_b = 2\mathbf{k}_p$. In our studies, we utilize phase-matching conditions to induce amplified SBS. This is done by modulating our input laser source by a frequency Ω_B in order to produce two counter propagating fields whose frequency interference was resonant with the phonon modes in our optical fiber.

Chapter 4

Methods

The two techniques used to measure and induce backwards SBS were an AC balance photodetection system and Coherent Anti-Stokes Brillouin Scattering (CABS) system. Both the AC balanced photodetection system and CABS were used to collect back the power amplification as described in chapter 3. We measured the phonon dissipation for a Ultra High Numerical Aperture (UHNA7) fiber, a photonic crystal fiber, and a tapered fiber at various temperatures to demonstrate and create a basis for TLS-phonon dynamic analysis. As described in section 2.2, TLS-phonon coupling has a relaxation and resonant absorption process that have unique temperature dependence's as seen in equations (2.15) and (2.16). This gives us a scalable relationship between the manner in which TLS's attenuate phonons in our samples. An extensive description of both experimental setups is given in next sections to illustrate the mechanism for measuring the phonon decay rates in optical fibers.

4.1 AC Balanced Photodetection

Our first method for performing amplified SBS was through an AC balanced photodetection(AC-BD) system and lock-in amplification. Our AC-BD system consists of a $1550nm$ laser source that is split into two counter propagating optical lines(pump and probe) and introduced into the optical fiber under detection(FUD). One arm of the split laser source passes through a polarization controller then through a phase modulator. The phase modulator is utilized to modulate our laser source into its carrier and Stokes/anti-Stokes sidebands at exactly Ω_B frequency away. The output light source is then sent through a band-pass filter to isolate a high-frequency sideband. This acts as our "pump" field. The second arm of the split laser source is sent through a Chopper in order to create an alternating signal at a frequency of $3000kHz$ that was used as a reference for the lock-in amplifier. This was done so that the lock-in amplifier could differentiate a component of the reference signal associated with the SBS power gain at that given frequency range. After the second arm passes through the Chopper it is split again into two arms, where one will act as an external probe field for the FUD and the other as a reference signal that has no interaction with the SBS process. A schematic of this is shown in figure 4.1.

Both pump and probe fields are the counter propagated through the FUD where they induce electrostrictive forces that cause an internal acoustic wave at frequency Ω. This acoustic wave acts as a Bragg grating that red shifts the pump field by the frequency of the mechanical wave. The frequency shift in our pump field causes a energy transfer from the pump to probe field when phase matching conditions are satisfied as shown in chapter 3.

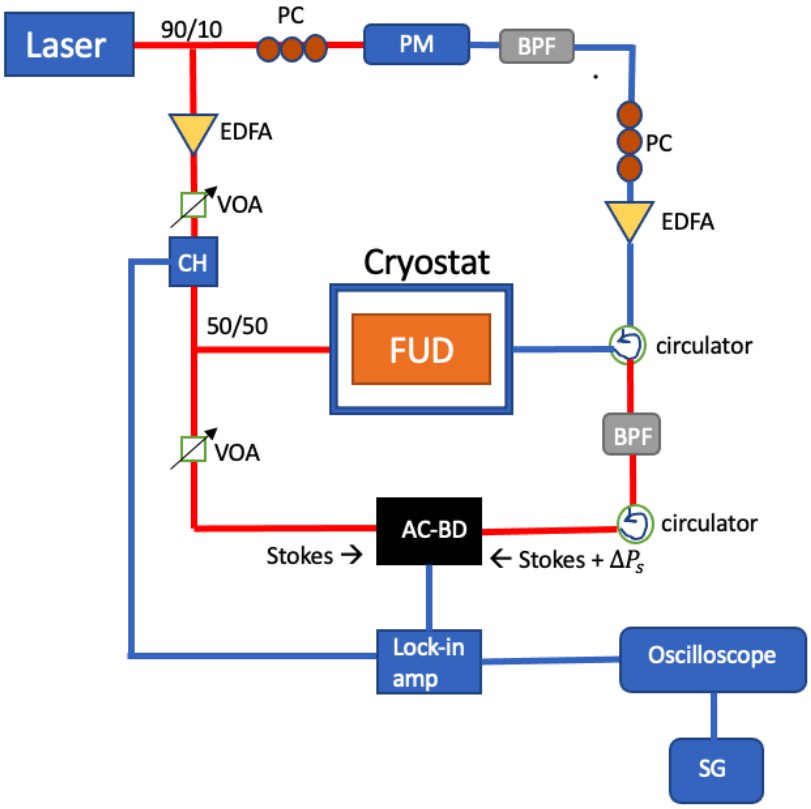

Figure 4.1: Experimental setup to measure amplified SBS using an AC balanced photodetector. The acronyms shown above stand for: EDFA - Erbium doped fiber amplifier, VOA - variable optical attenuator, PC - polarization control, AC-BD - balance detector, BPF - band pass filter, and PM - phase modulator. Our laser source is positioned at 1549.108 nm with max power. Our probe line is synthesized by sending pump laser light through a phase modulator that modulates incoming optical fields by 8.78 GHz. A temperature dependant BPF selects a Stokes side-band. Probe light is split in two arms, one acting as a reference and the other traversing the FUT. The power amplification of the Stokes beam line at Ω_B is acquired with lock-in detection.

This energy transfer is represented by a probe power amplification. Thus, the existing probe field is amplified by ΔP_s as written in equation (3.16). An illustration of this process is shown in figure 4.2. Once we have induced SBS the amplified probe signal is sent through a second band pass filter to ensure that we only collect light associated with the wavelength of our probe laser.

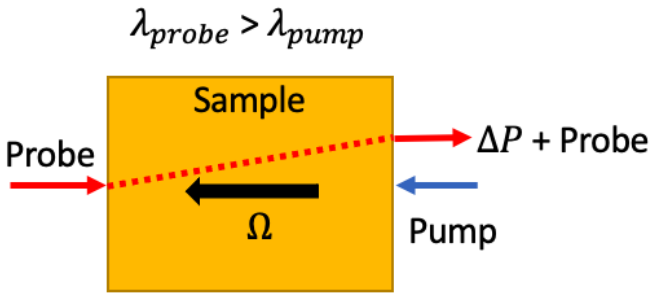

Figure 4.2: Schematic of amplified SBS in our sample. Probe and Pump are counter propagated into FUD which produces a beat tone. The co-propagating Probe and beat tone produce a lower frequency shift at exactly Ω_b and the counter-propagating pump and beat tone produce a higher frequency shift. This produced a red-shifted process that amplifies the Probe power by exactly the resonance frequency and a blue-shifted process for Probe-beat tone.

In order properly apply balanced photodetection, the reference signal associated with no SBS interaction passes through a variable optical attenuator in order to set its power equal to the amplified probe signal. This balanced source is then sent into one input photodiode of the AC-BD and the probe amplified signal is sent to the second input photodiode of the AC-BD. The AC-BD performs common mode rejection by positioning the two photodiodes in a serial-circuit causing a subtraction of their photocurrents and extracting any low signal noise. This difference is then sent to a transimpedance amplifier which produces a voltage output proportional to that difference. It is important to note that we use an AC version of the balanced photodetector in order to increase the suppression of any common fluctuations between the two optical inputs. A schematic of the AC-BD circuit is shown in Appendix A.

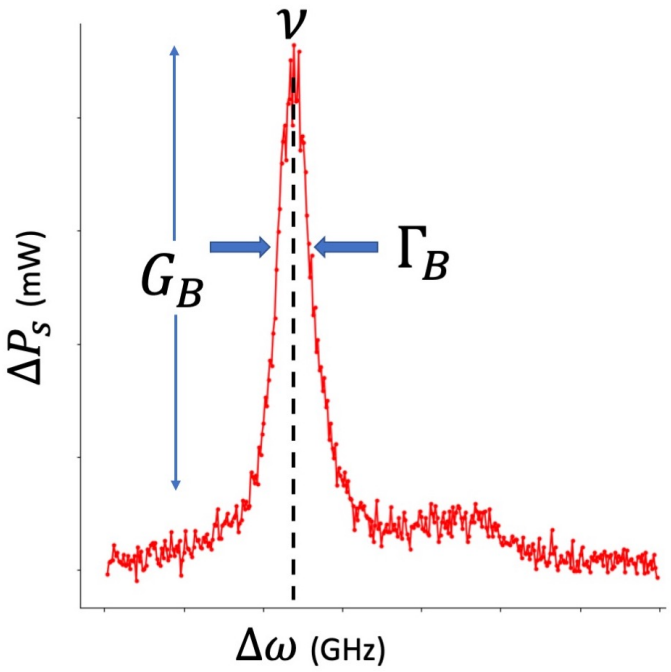

Figure 4.3: Illustration of power amplification response due to SBS. The collected power amplification takes the form of a Lorenzian, where the height is proportional to the Brillouin gain, the center frequency gives back the speed of sound in the material, and the FWHM gives back the phonon dissipation rate

The AC-BD then subtracts the reference signal with the probe amplified signal and recovers ΔP_s. This information is sent through a lock-in amplifier to amplify ΔP_s and send it through an oscilloscope where we collect all the power associated with the Brillouin gain as a function of time. In order sync the capture between ΔP_s to the phonon resonance frequency, the modulated frequency used to create the pump field is swept across different frequencies resulting in a Lorentzian response of ΔP_s. An example of this signal is illustrated in figure 4.3. To calibrate the time response of the frequency sweep with capture of our signal we used an external signal generator(SG) that was used as a trigger for the frequency sweep. This was done so that whenever we had a rising signal coming from our SG we were able to detect a voltage on our oscilloscope proportional to the frequency sweep. Once a signal was accumulated we were able to fit the power spectra with equation (3.16) and retrieve the full width-half-max (FWHM).

4.2 Coherent Anti-Stokes Brillouin Scattering

In our data collection process we introduced coherent anti-Stokes Brillouin scattering(CABS) to measure the phonon decay rates of the optical fiber, UHNA7. CABS was used as the primary source to do phonon spectroscopy for our optical samples due to its high signal sensitivity down to fW signals. CABS works by implementing a four-wave mixing technique that performs both SBS and heterodyne spectroscopy. CABS utilizes a pump-probe setup similar to that described in the AC-BD system, where a laser source (pump) is split into two optical lines to facilitate amplified SBS. The one arm passes through an intensity modulator where the output is sent through a tunable band pass filter to isolate a Stokes sideband. A schematic of how the intensity modulator works is added in appendix A for further understanding. This Stokes side band acts as our probe Stokes field to induce SBS. Before counter propagating pump and Stokes fields into the FUD, each field passes through two separate polarization beam splitters(PBS) in order to co-polarize each field and negate passage of pump/Stokes signal into the detector.

Once passed through the PBS, Stokes and pump fields are counter propagated into FUD, which induces an acoustic field amplification as described in the previous section. Here the amplified sound waves are coupled with an external laser source denoted as Probe. The second laser source is positioned at a wavelength that can be distinguished from the probe laser wavelength. The probe light then couples with the stimulated phonons. The coupling of the Probe and stimulated phonons produce a Stokes backscatter whose frequency is equal to the difference between phonon frequency and probe frequency. The Stokes backscatter is guided through a circulator that then photo-mixes with a local oscillator to produce a photocurrent proportional to the phonon frequency, Ω_B. This is well known as a heterodyne process where two optical inputs are photo-mixed in order to produce a detectable radio frequency for modern electronics.

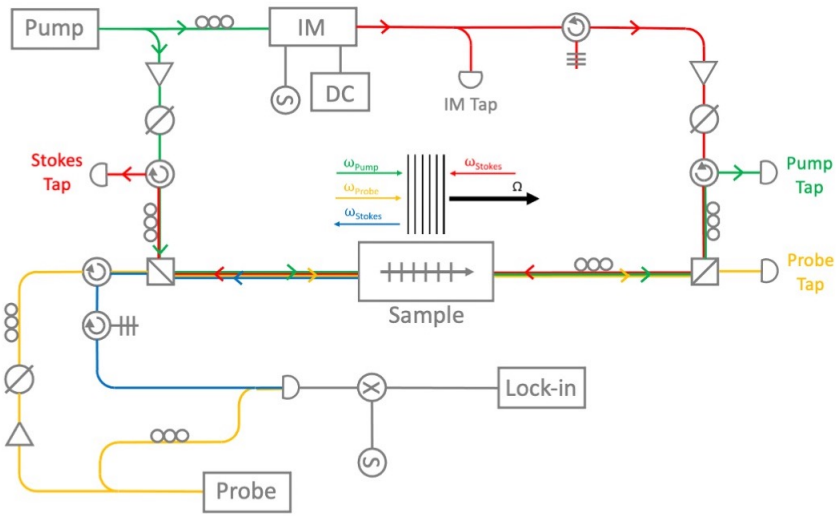

Figure 4.4: Experimental setup of CABS used to measure power amplification induced from SBS in UHNA7. laser source is positioned at 1549 nm range wavelenghts that are dependent on materials phonon resonance frequency and sample lenght. Pump-probe schematic is used where Stokes field is synthesized by sending pump laser light through an intensity modulator that is positioned at Ω_B. The carrier and the high frequency side-band are removed by operating at the null point bias point of the IM and band-pass filtering. Pump and Stokes fields are counter-propagated into sample to produce a acoustic waves which will then couple with the external probe field. Probe-acoustic wave produce a Stokes backscatter at resonance frequency that is photomixed with a LO and sent for detection through a lock-in amplifier.

The final steps are to then read the photocurrent through a photodetector where the signal passes through a lock-in amplifier and measures a voltage output. In order to accurately measure the resonance Stokes scatter, we sweep the modulated pump signal by the Brillouin resonance frequency and acquire a Lorentzian power spectrum at the lock-in stage. The final output is then the power as a function of the Brillouin resonance sweep that is proportional to the information shown in figure 4.3. Given that TLS-phonon coupling is a temperature dependent process, we ran these measurements at cryogenic temperatures within 800mK to 10K at 1K intervals. The temperature of the FUD was controlled using a Dry Ice 0.9K cryostat. This was done by splicing the FUD into the CABS set up and locating that splice onto the oxygen-free copper plate of the 1K stage in the cryostat. A holder was designed

to assure contact between the copper plate with our fiber and reduce cooling loss. The system was cooled down using Helium gas which was introduced into the outer layer of cryostat(4K stage) then condensed via pressure control. Once the required temperature for the 4K stage was acquired, a single shot process was implemented to achieve base temperature(800mK-1K) in the 1K stage.

Measurements were taken by inducing amplified SBS in CABS while the FUD was at base temperature, then collecting back the power spectrum signals as the cryostat warmed up. In addition, base temperature was maintained while we modulated the input pump-Stoke power between 1-130mW at 10mW intervals in order to find the critical acoustic intensity needed to saturate resonant absorption.

Chapter 5

Results

The samples chosen for this study consisted of a tapered fiber, a photonic crystal fiber (PCF), and a UHNA7 optical fiber. The tapered fiber and PCF were specifically chosen to showcase confinement. An illustration of each fiber is shown in figure 5.1 with dimension specifications. In order to acquire the frequency range in which to sweep the pump field modulation for optimal SBS power amplification, preliminary power spectra measurements were obtained for UHNA7, the PCF, and a tapered fiber at room temperature. We show the power spectra for the PCF in figure 5.2, which was collected using the AC balanced photodetection set up and in figure 5.3 we show the power spectra collected for a tapered fiber at room temperature.

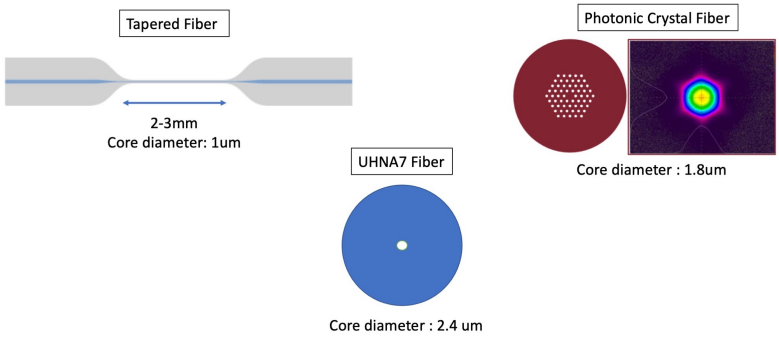

Figure 5.1: Illustration of tapered fiber, photonic crystal fiber, and UHNA7 fiber used in TLS acoustic dynamics study. Core diameter is defined for each fiber.

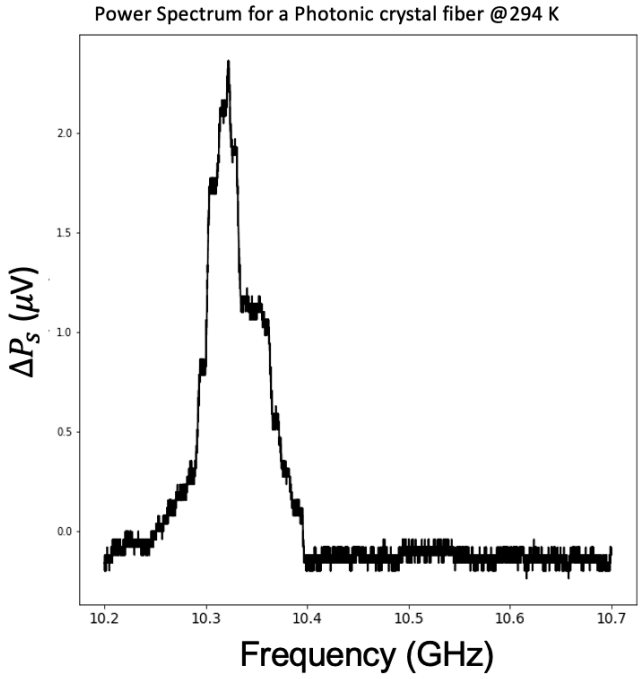

Figure 5.2: Power spectra as a function of frequency for photonic crystal fiber taken at room temperature

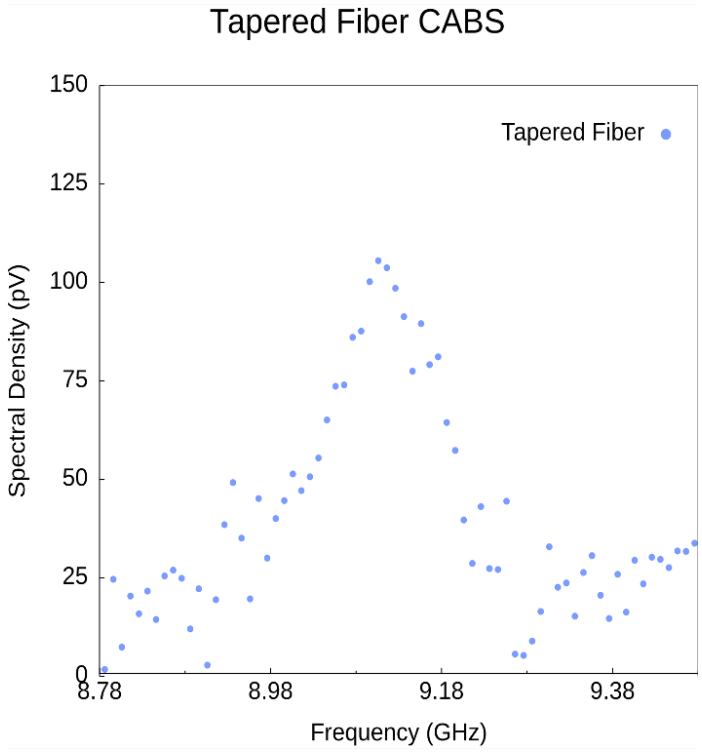

Figure 5.3: Power spectra as a function of frequency for tapered fiber taken at room temperature

Power spectra measurements were collected for UHAN7 at 800mK, 1.2K, and 5-9K temperatures using the CABS set up as a simple test-bed to study TLS dynamics. In figure 5.4, we show the power spectrum of UNHA7 at 800mK fitted by the equation (3.16). By fitting our signal with ΔP_s, we are able to correlate the FWHM (linewidth) to the phonon dissipation rate, Γ [29]. This was done for all power spectra collected at various temperatures. The main objective of these measurements are to plot the linewidth as a function of increasing cryogenic temperatures. By doing so, we employ a method for analyzing phonon dissipation produced from TLS-phonon coupling. In our findings we observed acoustic attenuation originating from relaxation absorption and overall provide the building blocks to continue these studies for confined systems.

The main mechanisms for phonon dissipation in amorphous material at cryogenic temperatures is through resonant and relaxation absorption induced from TLS-phonon coupling. Resonant absorption has unique dynamics that are dependent on temperature and acoustic field intensities. This is given by reference [19] :

$$\Gamma_{res} = \left(\frac{\pi P \gamma_l^2 \Omega}{\rho v^2} \right) \frac{\tanh\left(\frac{\hbar\Omega}{2k_B T}\right)}{\sqrt{1 + \frac{J}{Jc}}}. \tag{5.1}$$

This equation can be derived from α_{res}, where P is the TLS density of state, γ_l is the deformational potential for longitudinal phonon modes, ρ is the mass density of the core of the fiber, T is the temperature of the system, Ω is the phonon resonance frequency, and v_l is the longitudinal speed of sound. The factor $\frac{J}{Jc}$ takes into consideration the effects of the acoustic field intensities and gives rise to saturation of resonant absorption.

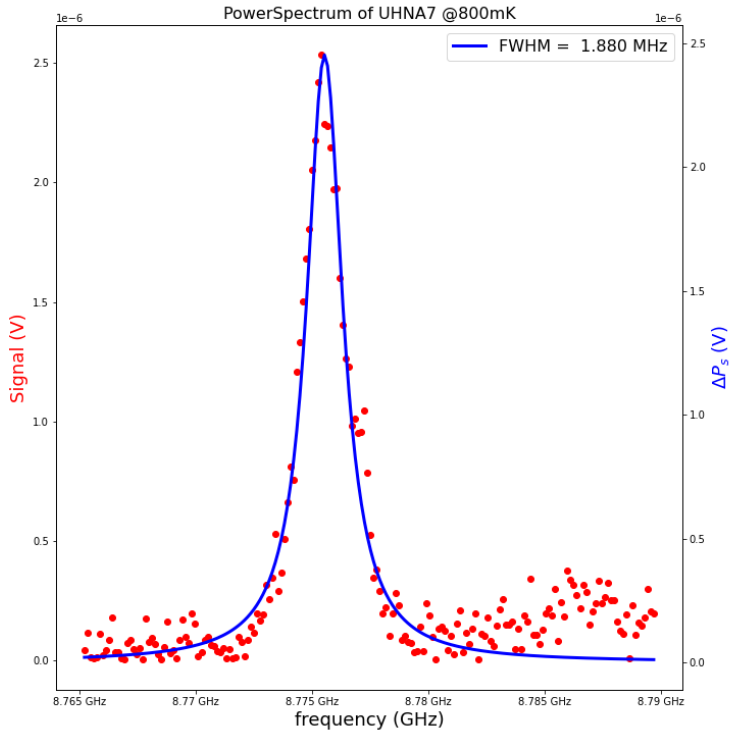

Figure 5.4: Amplified SBS power spectrum for UHNA7 taken at 800mK. Red dots represent signal which are fit with equation 3.14 given by blue fit.

At high enough temperatures ($k_BT \ggg \hbar\Omega$) TLS's are said to have equal rates of absorbing and emitting phonons, thus stimulated phonon emission coherently amplifies acoustic fields and resonant absorption is suppressed. At low temperatures ($k_BT \lll \hbar\Omega$) and low acoustic intensities, the TLS is said to resonantly absorb a phonon and decay via spontaneous phonon emission that attenuate the incident acoustic field.

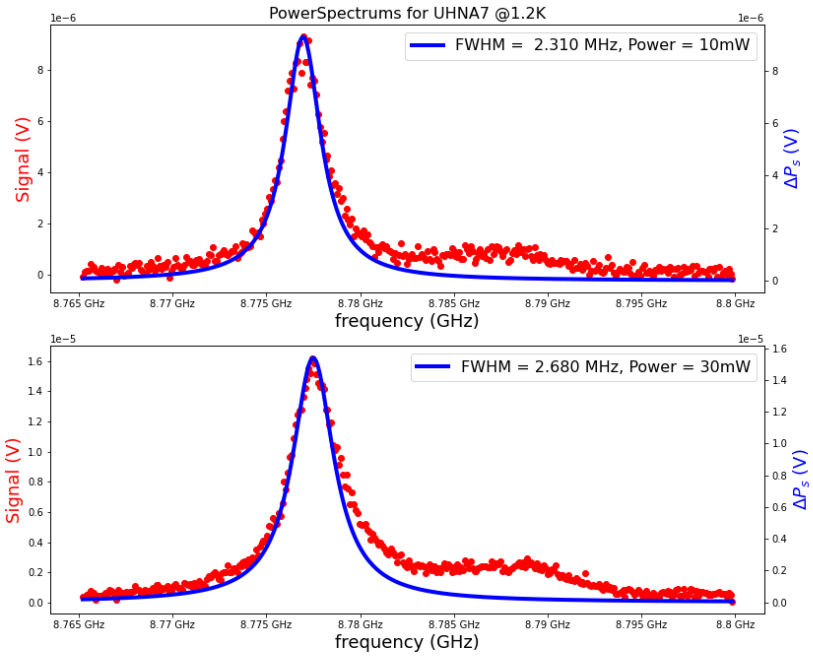

Figure 5.5: **Top**: Amplified SBS power spectrum for UHNA7 taken at 1.2K and 10 mW optical input powers. **Bottom**: Amplified SBS power spectrum for UHNA7 taken at 1.2K and 30 mW optical input powers. Red dots represent signal which are fit with equation (3.16) given by blue fit.

In order to observe resonant absorption and saturation of resonant absorption, measurements of ΔP_s were taken at 1.2K for pump and Stokes powers between 1-90mW at intervals of 10mW. This was done to investigate what critical power induced saturation of resonant absorption and to see if we retrieved a reduction of the linewidth for higher input powers. Since the pump and Stokes powers produce the intensity of our induced beat note (phonons), by changing the powers used for both pump and Stokes optical fields we are proportionally changing the acoustic intensity. Unfortunately in the process of increasing the pump and Stokes fields we were not able to observe resonant absorption since an increase in the linewidth was acquired rather than a decrease. This can be seen in figure 5.5, where equation (3.16) is plotted over two retrieved signals at 1.2K for 10mW and 30mW pump and Stokes powers.

The FWHM (linewidth) increases from 2.31 MHz to 2.68 MHz, indicating that we are not seeing saturation of resonant absorption. In addition, we increased pump and Stokes powers in intervals of 10mW from 1-90mW. The increase in linewidth as powers increased and the shift in center frequency shown in figure 5.6 alluded to heating in the core of UHNA7.

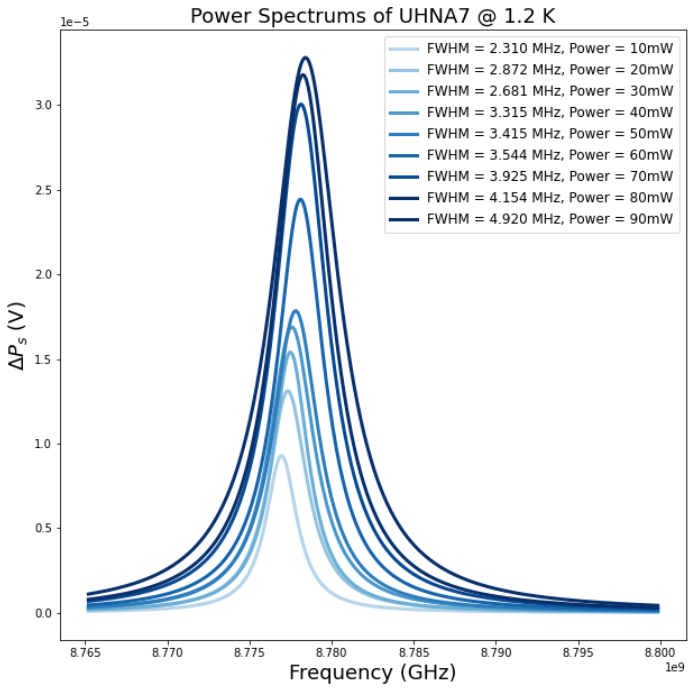

Figure 5.6: Power transfer fits for UHNA7 at 1.2K for pump and stokes input powers between 10mW-90mW. Cryogenic temperature was kept at base temperature as input power were increased in intervals of 10mW.

Relaxation absorption is another form of TLS acoustic attenuation that originates from external strain field perturbations. These external strain fields can take the form of time varying acoustic or electric fields that perturb the TLS tunneling state energy. This process brings the TLS in and out of thermal equilibrium which in return causes a relaxation process in order to return the TLS back to equilibrium. Thus, a TLS can absorb energy from a phonon and emit that energy into its environment. This

then induces phonon dissipation in the form of [19] :

$$\Gamma_{rel} = \frac{\pi^3 P \gamma_l^2}{24 \rho^2 v_n^2 \hbar^4} \left(\sum_n \frac{\gamma_l^2}{v_l^5} \right) (k_B T)^3 \,. \tag{5.2}$$

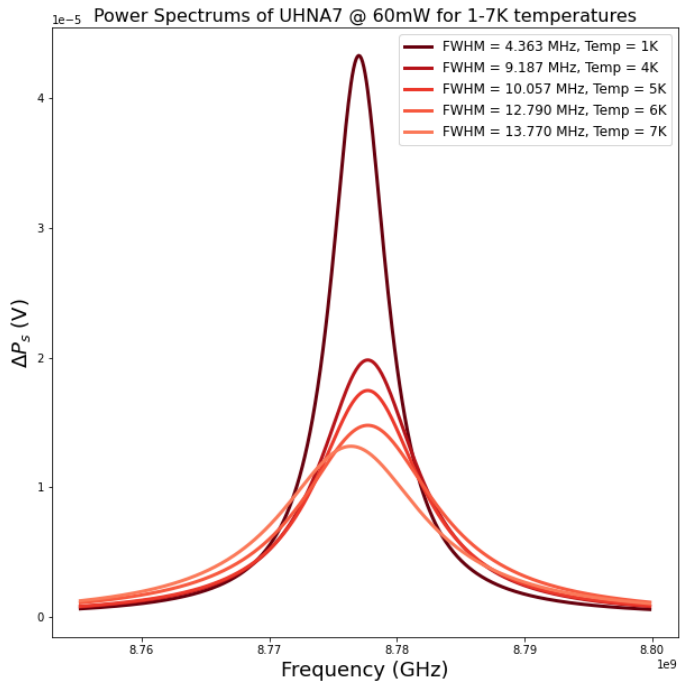

Figure 5.7: Power transfer fits for UHNA7 at 1-7K temperatures. Probe was kept at 10mW while Pump and Stokes were kept at about 60mW.

Phonon dissipation from TLS relaxation absorption arises from the elastic modulus shown in equation (2.14). The key characteristic of equation (5.2) is the temperature cubed law dependence. This factor is a key marker for distinguishing relaxation absorption from resonant absorption. Comparing equation 5.1 and 5.2 we note that resonance absorption becomes acute at low temperatures whereas relaxations absorption dominates as cryogenic temperatures increase. We show this in figures 5.7 and 5.8 where we see the phonon dissipation rate (linewidth) increase as we advance to higher cryogenic temperatures. In addition, we also make note of the center frequency

shift as we increase temperatures. This is a known response described by reference [12] as:

$$
\begin{aligned}
(\Delta\omega(T) - \Delta\omega(T_o))_{res} &= -\frac{P\gamma_l^2}{\rho v} \ln\left(\frac{\hbar\Omega}{k_B T}\right) \quad , \\
(\Delta\omega(T) - \Delta\omega(T_o))_{rel} &= -\frac{P\gamma_l^2}{\rho v^2}\frac{3}{2} \ln\frac{T}{T_o}.
\end{aligned}
\tag{5.3}
$$

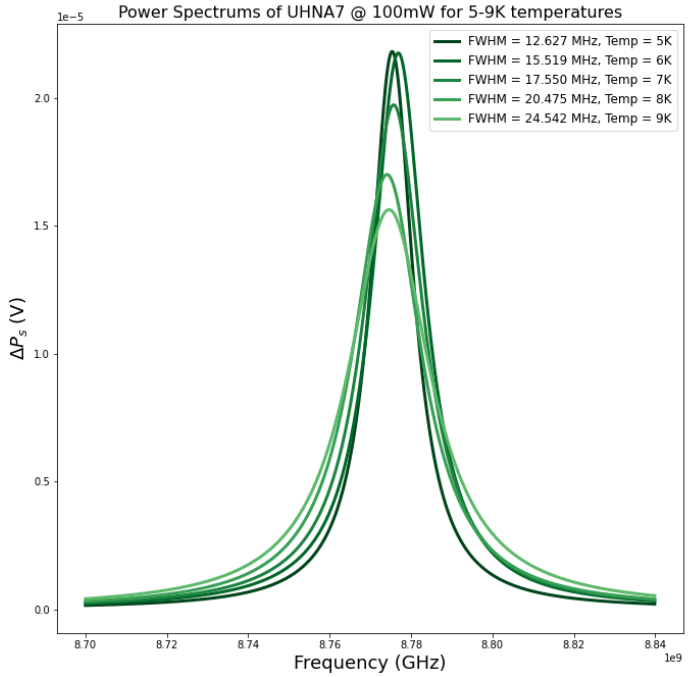

Figure 5.8: Power transfer fits for UHNA7 at 5-9K temperatures. Probe was kept at 10mW while Pump and Stokes were kept at about 100mW.

In order to prove that we were seeing relaxation absorption in figures 5.7 and 5.8, we fit the linewidth as a function of temperature with equation (5.2). Given the knowledge that the core of our fiber is doped with germanium, we account for background phonon losses coming from Rayleigh scattering, phonon-phonon scattering, imperfect guiding, and possibly in-homogeneous broadening [19]. Thus, when fitting equation (5.2) to our linewidth measurements we add an offset value. Our results

are shown in figure 5.9, where we fit the linewidth measurements with a temperature cubed power law and a Γ_{offset} of 10.85 MHz for temperatures between 5-9K. When measuring the correlation between our linewidth measurements and the TLS relaxation phonon decay rate, we found a Pearson correlation of 0.996. Given the correlation between $\Gamma_{rel} + \Gamma_{offset}$ and our linewidth measurements, we are able to conclude that contribution to the phonon dissipation in UHNA7 originate from TLS relaxation absorption. In addition, by fitting Γ_{rel} to our linewidth measurements we retrieved a P value of 0.95 eV or $14 * 10^{44}(J^{-1}m^{-3})$, which is a reasonable result for UHNA7 [19]. We also fit Γ_{rel} to our linewidth measurements for temperature between 1-7K, however equation (5.3) did not suffice to represent the phonon dissipation in UHNA7 at temperatures between 1-7K.

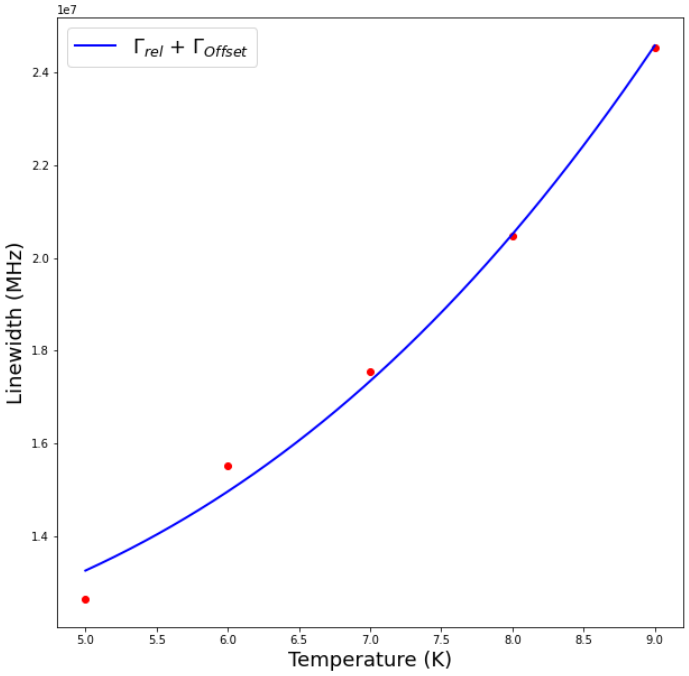

Figure 5.9: Linewidth measurements taken from equation 3.14 fit as a function of temperature. Relaxation phonon decay rate function 5.2 is fitted on top with an acoustic loss offset.

The use of Brillouin spectroscopy for studying TLS dynamics in amorphous material demonstrated to be a solid foundation for understanding how we can observe acoustic attenuation induced resonant and relaxation absorption.The power spectra measurements captured using CABS at cryogenic temperatures resulted in phonon dissipation arising from relaxation absorption that followed the expected temperature power law as described in reference [7; 12]. We found the lowest phonon dissipation rate in UHNA7 to be 1.5MHz at 800mK and the largest dissipation of 24MHz at 9K.

Chapter 6

Conclusion

We found that stimulated Brillouin scattering is sufficient for analysing TLS phonon dynamics in optomechanical systems such as optical fibers. This is due to the notable coherent acousto-optic coupling and its precision spectroscopy that SBS offers [14; 15; 17]. We found that the phonon dissipation in UHNA7 can be described by the TLS model at low cryogenic temperatures. The results found in chapter 5 work as a testing-ground for building a technique to measure TLS dynamics in optical fibers at Northern Arizona University, which will allow for future studies of TLS dynamics in confined systems.

Future directions for this work include measuring power spectrum's for a photonic crystal fiber and a tapered fiber at low cryogenic temperatures. The objective of these measurements is to see if we observe alterations of the phonon dissipation rate (linewidth) that correspond to the trend of relaxation or resonant absorption for confined systems as described in equation (2.18). Overall, the work presented in this thesis contributes to the ongoing experimental work in trying to uncover TLS behaviors in confined systems and the beginning steps for understanding the microscopic properties of glasses at cryogenic temperatures.

Appendix A

Supplement Figures

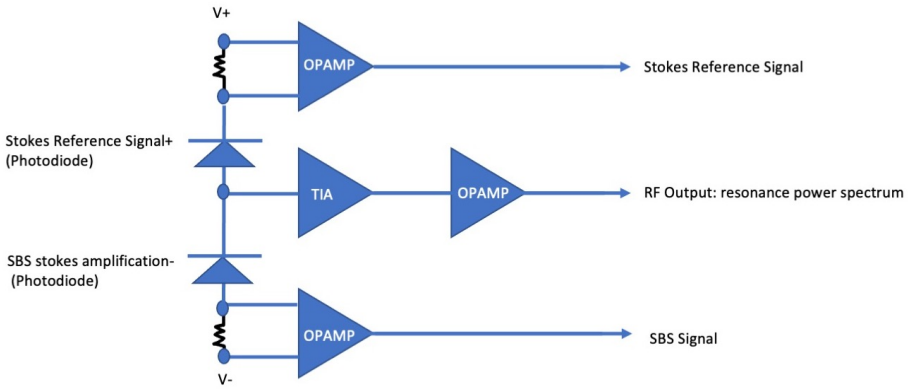

Figure A.1: An illustration of circuit structure inside an AC Balanced photodetector. Left side of circuit represents two photodiodes put in a parallel serial circuit, where each input is sent through an operational amplifier to offer single side analyzing. The subtracted voltage passes through the TIA or transimpedance amplifier where the photocurrent is converted to a voltage signal proportional to the subtracted signals(low-noise)

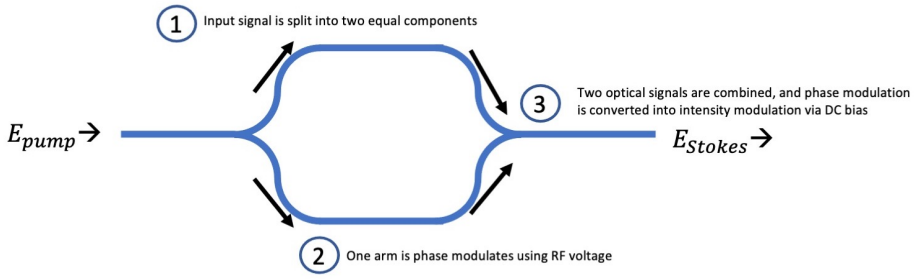

Figure A.2: Illustration of optical input through an intensity modulator. Here, input electric field passes through two separate beam spliters that split and recombine at end of system. One arm is phase modulated using an RF voltage and then converted into intensity information using a DC voltage. The output electric field is then modulated by a manually set RF voltage.

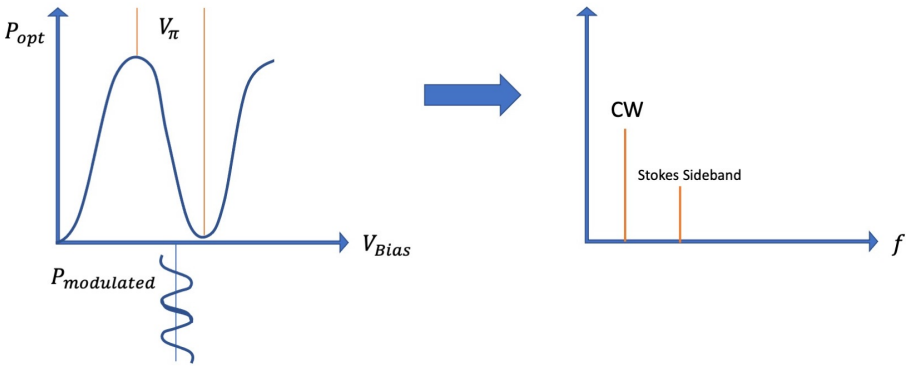

Figure A.3: Visual representation of intensity modulation using a RF voltage and DC voltage bias that gives back carrier wave and Stoke or anti-Stoke sidebands.

Bibliography

[1] M. H. Devoret and R. J. Schoelkopf. Superconducting circuits for quantum information: An outlook. *Science*, 339(6124):1169–1174, Mar 2013.

[2] Aaron O'connell, M Ansmann, R Bialczak, M Hofheinz, N Katz, Erik Lucero, C Mckenney, M Neeley, H Wang, E Weig, A Cleland, and J Martinis. Microwave dielectric loss at single photon energies and millikelvin temperatures.

[3] R. W. Simmonds, K. M. Lang, D. A. Hite, S. Nam, D. P. Pappas, and John M. Martinis. Decoherence in josephson phase qubits from junction resonators. *Phys. Rev. Lett.*, 93:077003, Aug 2004.

[4] Serge Galliou, Maxim Goryachev, Roger Bourquin, Philippe Abbé, Jean Pierre Aubry, and Michael E. Tobar. Extremely low loss phonon-trapping cryogenic acoustic cavities for future physical experiments. *Scientific Reports*, 3(1), Jul 2013.

[5] Cesar Seoanez, Francisco Guinea, and H Castro. Dissipation due to two-level systems in nano-mechanical devices. *EPL*, 78(6):60002–60002, Jun 2007.

[6] Markus Aspelmeyer, Tobias J. Kippenberg, and Florian Marquardt. Cavity optomechanics. *Reviews of Modern Physics*, 86(4):1391–1452, Dec 2014.

[7] Ryan O Behunin, Francesco Intravaia, and Peter T Rakich. Dimensional trans-

formation of defect-induced noise, dissipation, and nonlinearity. *Physical review*, 93(22), Jun 2016.

[8] T. Kamppinen, J. T. Mäkinen, and V. B. Eltsov. Dimensional control of tunneling two-level systems in nanoelectromechanical resonators. *Physical Review B*, 105(3), Jan 2022.

[9] Adam D Alfieri, Surendra B Anantharaman, Huiqin Zhang, and Deep Jariwala. Nanomaterials for quantum information science and engineering. *Advanced Materials*, page 2109621–2109621, Feb 2022.

[10] O. Astafiev, Yu. Pashkin, Y. Nakamura, T. Yamamoto, and J. Tsai. Quantum noise in the josephson charge qubit. *Physical Review Letters*, 93(26), Dec 2004.

[11] O. Astafiev, Yu. A. Pashkin, Y. Nakamura, T. Yamamoto, and J. S. Tsai. Quantum noise in the josephson charge qubit. *Phys. Rev. Lett.*, 93:267007, Dec 2004.

[12] W A Phillips. Two-level states in glasses. *Reports on Progress in Physics*, 50(12):1657–1708, Dec 1987.

[13] Siegfried Hunklinger and Manfred von Schickfus. Acoustic and dielectric properties of glasses at low temperatures. *Topics in current physics*, page 81–105, Jan 1981.

[14] Paulo Dainese, Russell, Nicolas Joly, Jonathan Knight, Gustavo S Wiederhecker, Hugo L Fragnito, Vincent Laude, and Abdelkrim Khelif. Stimulated brillouin scattering from multi-ghz-guided acoustic phonons in nanostructured photonic crystal fibres. *Nature Physics*, 2(6):388–392, Jun 2006.

[15] Wenjun Qiu, Peter T Rakich, Heedeuk Shin, Hui Dong, Marin Soljacic, and Zheng Wang. Stimulated brillouin scattering in nanoscale silicon step-index

waveguides: a general framework of selection rules and calculating sbs gain. *Optics Express*, 21(25):31402–31402, Dec 2013.

[16] Prashanta Kharel, Ryan O Behunin, William H Renninger, and Peter T Rakich. Noise and dynamics in forward brillouin interactions. *Physical review*, 93(6), Jun 2016.

[17] Benjamin J Eggleton, Christopher G Poulton, Peter T Rakich, Michael J Steel, and Gaurav Bahl. Brillouin integrated photonics. *Nature Photonics*, 13(10):664–677, Oct 2019.

[18] Ryan O Behunin, Parashu Kharel, William H Renninger, and Peter T Rakich. Engineering dissipation with phononic spectral hole burning. *Nature Materials*, Jun 2016.

[19] Behunin R O, P Kharel, Renninger W H, H Shin, F Carter, E Kittlaus, and Rakich P T. Long-lived guided phonons in fiber by manipulating two-level systems, 2015.

[20] R. C. Zeller and R. O. Pohl. Thermal conductivity and specific heat of noncrystalline solids. *Physical Review B*, 4(6):2029–2041, Sep 1971.

[21] R. O. Pohl. Low temperature specific heat of glasses. *Topics in Current Physics*, page 27–52, 1981.

[22] Clare C Yu. Interacting defect model of glasses: Why do phonons go so far? *Physical Review Letters*, 63(11):1160–1163, Sep 1989.

[23] B Golding and J E Graebner. Relaxation times of tunneling systems in glasses. *Topics in current physics*, page 107–134, Jan 1981.

[24] W A Phillips. Tunneling states in amorphous solids. *Journal of Low Temperature Physics*, 7(3-4):351–360, May 1972.

[25] A. Abragam. *The Principles of Nuclear Magnetism*. International series of monographs on physics. Clarendon Press, 1961.

[26] Jiansong Gao, Jonas Zmuidzinas, Benjamin A. Mazin, Henry G. LeDuc, and Peter K. Day. Noise properties of superconducting coplanar waveguide microwave resonators. *Applied Physics Letters*, 90(10):102507, Mar 2007.

[27] C. Seoánez, F. Guinea, and A. H. Castro Neto. Dissipation in graphene and nanotube resonators. *Physical Review B*, 76(12), Sep 2007.

[28] C. Seoánez, F. Guinea, and A. H. Castro Neto. Surface dissipation in nanoelectromechanical systems: Unified description with the standard tunneling model and effects of metallic electrodes. *Physical Review B*, 77(12), Mar 2008.

[29] R.W. Boyd. *Nonlinear Optics*. Elsevier Science, 2020.